Opto-Electronic Advances

Supplementary information

November 2023, Vol. 6, No. 11

DOI: 10.29026/oea.2023.230018

Spatiotemporal hemodynamic monitoring via configurable skin-like microfiber Bragg grating group

Hengtian Zhu[1†], Junxian Luo[2†], Qing Dai[3†], Shugeng Zhu[1], Huan Yang[1], Kanghu Zhou[1], Liuwei Zhan[1], Biao Xu[3], Ye Chen[1], Yanqing Lu[1] and Fei Xu[1*]

[1]College of Engineering and Applied Sciences and Collaborative Innovation Center of Advanced Microstructures, Nanjing University, Nanjing 210023, China; [2]School of Physics, Nanjing University, Nanjing 210023, China; [3]Department of Cardiology, Affiliated Drum Tower Hospital, Medical School of Nanjing University, Nanjing 210008, China.

[†]These authors contributed equally to this work.

*Correspondence: Fei Xu, E-mail: feixu@nju.edu.cn

This file includes:

Supplementary information for this paper is available at https://doi.org/10.29026/oea.2023.230018

Section 1: Materials and methods

Fabrication of the skin-like μFBG patch

The fabrication of a soft μFBG patch includes the precise tapering technology, flexible packaging technology, and advanced femtosecond laser direct-writing technique. The detailed preparation process is illustrated in Supplementary Fig. S1. First, the microfiber was tapered by a standard commercial single-mode fiber (with a diameter of 125 μm) using the flame brushing method. The diameter of the microfiber was controlled at 12 μm. The transition region of the tapered fiber was smooth and had a uniformly varying diameter guaranteed by the flame brushing method. Second, the microfiber was encapsulated by PDMS (Base: Curing agent = 10:1) by scraper coating on a glass slide, forming a thin and soft patch. Third, FBG was inscribed noninvasively in the optical microfiber by a femtosecond laser (Pharos, Light-conversion). The grating period was 1.075 μm, which was controlled by a high-precision translation stage so that the working wavelength of the μFBG was 1555 nm. The working wavelength of the μFBG can be adjusted by different grating spaces when the microfiber's diameter is fixed. After inscribing the FBG, the soft μFBG patch was detached from the glass slide.

Stress/Vibration response test

The stress response and vibration response were characterized by a homemade stress test equipment, which is shown in Supplementary Fig. S2. A thick Ecoflex (smooth-on 00-30) substrate was used to simulate human skin. When testing the stress response, the PC controlled the translation stage by moving up and down to compress the soft μFBG patch using an Ecoflex contactor, resulting in different degrees of deformation. Optical signal acquisitions such as OSA (Yokogawa AQ6370C) and FBG interrogator (Smart Fibres Ltd. SmartScan) detected the reflective spectrum and wavelength shift of the soft μFBG patch in real time. A force meter was used to calibrate the compression force. The same test method was used to characterize the stress response of commercial FBGs with diameters of 80 μm and 125 μm. When testing the vibration response and conducting the repetition test, a vibrostand was employed to apply stress on the soft μFBG patch at different frequencies controlled by a signal generator. The FBG interrogator recorded the wavelength shift at the same time.

Acquisition, processing, and analysis of BCG and pulse

An FBG interrogator was employed to record the wavelength shift of the soft μFBG patch caused by micro stress on the skin surface due to cardiovascular activity with a sampling frequency of 2500 Hz. The subjects were instructed to relax their bodies and to remain calm during the measurement. When detecting the BCG signal, the soft μFBG patch was attached to the chest skin at the tricuspid site. Apply a small amount of medical alcohol to the surface of the skin, and use the tension of the alcohol to make the PDMS patch adhere conformally to the skin surface. After the alcohol evaporated, the patch would maintain close contact with the skin. By employing the short-time Fourier transform (STFT), the time-frequency diagrams of the raw BCG signal and raw pulse wave were obtained. The frequency components related to heart rate were clearly identified in the time-frequency diagram. A 3–15 Hz bandpass filter was employed to eliminate the low-frequency respiration signal and the high-frequency noise. After filtering, the BCG signal containing the feature of cardiovascular activity was obtained. The I wave, which represents the beginning of cardiac ejection, was extracted according to the minimum point within one cardiac cycle. When detecting the pulse wave, the soft μFBG patch was attached to the skin at the superficial artery sites. Also, medical alcohol was employed to ensure the tight adhesion. A 0.5–10 Hz bandpass filter was employed to remove the baseline shift caused by the movement of the arm and wrist and high-frequency noise. After filtering, B wave, which also represents the beginning of cardiac ejection, was extracted according to the closest minimum point before the systolic peak within one cardiac cycle. Heart rate was calculated according to the time interval of the above feature point.

PTT calculation

To analyze the propagation process of the pulse wave and calculate the PTT, the soft μFBG group was built by connecting two μFBG patches in series. One soft μFBG patch was attached to the chest skin at the tricuspid site to detect the BCG signal, and the other was attached to the skin at the superficial artery sites to detect pulse waves. An FBG interrogator was employed to record the wavelength shift of soft μFBG patches with a sampling frequency of 2500 Hz. The BCG

signal and pulse wave were well time synchronized. After signal preprocessing, the feature points of the BCG signal and pulse wave (I wave and B wave), which represent the beginning of cardiac ejection, were extracted. Then, PTT was calculated according to the time interval between the I wave and B wave. Mean PTT was calculated to demonstrate the PTT validation at different propagation routes (Fig. 4(h)) and the PTT fluctuation during exercise (Fig. 5(d) and Supplementary Fig. S8). The PTT of every cardiac cycle was present when monitoring PR to demonstrate the dynamic monitoring capability.

The detection site of BCG signal was fixed on the chest skin at the tricuspid site. The site of the pulse wave depended on the required propagation route. When calculating systemic PTTs, CA, RA, and PA were chosen as the sites of pulse waves. When monitoring hemodynamic parameters during exercise, PA was chosen as the site of pulse wave. When monitoring PR, RA was chosen as the site of the pulse wave.

Analytical model of the artery

A theoretical artery model[S1] was established to relate the PTT to BP and PR for continuous and noninvasive hemodynamic monitoring. Supplementary Fig. S9 shows a schematic diagram of the artery model. The pulse wave propagates along the artery wall in the direction x. The artery is idealized as a thin walled, straight and flexible cylinder tube. The length, radius, and thickness of the artery are L, r, and h, respectively. The internal pressure (also known as BP) and external pressure are vertically applied on the artery wall, resulting in the transmural pressure P ($= P_{\rm bp} - P_{\rm ex}$). P and the stress σ in the circumferential direction meet the balance condition of force. The relationship between the transmural pressure P and PWV ($= L/PTT$) is represented by the following equation:

$$P = be^{-\left(\frac{k}{PWV}\right)},$$

b and k are undetermined coefficients relative to the individual.

The above equation explains the PTT fluctuation during exercise. Due to the increased BP caused by the contraction of nonexercise muscle blood vessels in exercise, the transmural pressure P was increased, resulting in accelerated PWV and shortened PTT. Additionally, when monitoring PR, the transmural pressure P was decreased due to the rising external pressure caused by the inflatable cuff, resulting in the rapidly increasing PTT.

Section 2: Supplementary figures

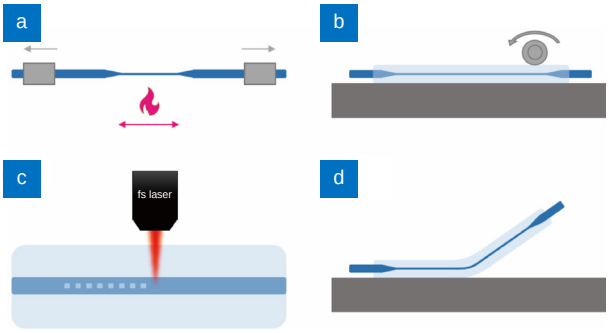

Fig. S1 | Preparation process of soft μFBG patch. (**a**) Tapering of optical microfiber by the flame brushing method. (**b**) A thin PDMS film is dip coated to encapsulate the microfiber on a glass slide. (**c**) FBG is inscribed non-invasively in the optical microfiber by femtosecond laser direct writing technique. (**d**) Soft μFBG patch is detached from the glass slide.

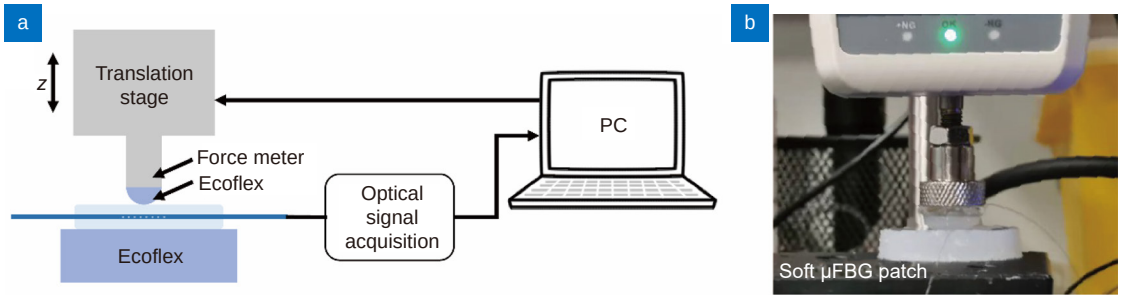

Fig. S2 | Stress test equipment. Schematic diagram (**a**) and photograph (**b**) of the stress test equipment.

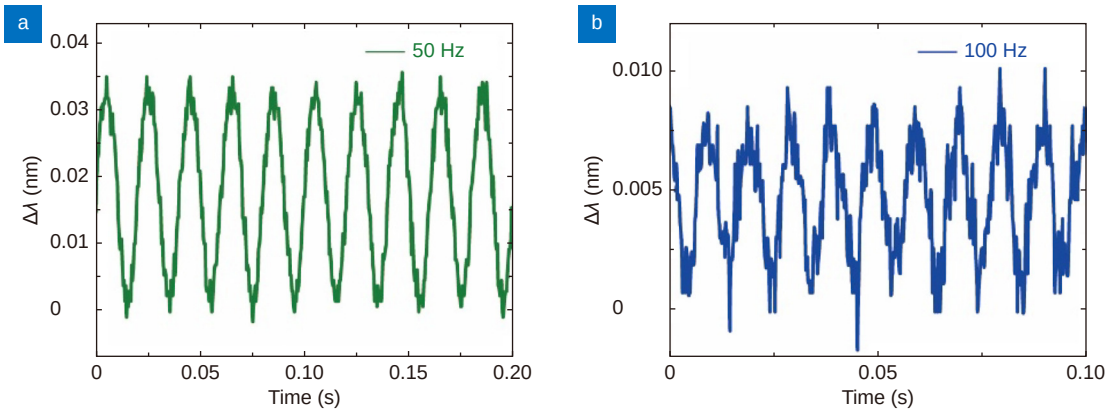

Fig. S3 | Vibration test. Vibration characterization of the soft μFBG patch under frequencies of 50 Hz (**a**) and 100 Hz (**b**). The 100 Hz vibration signal has a weak amplitude and a low SNR due to limitations in the performance of the vibrostand.

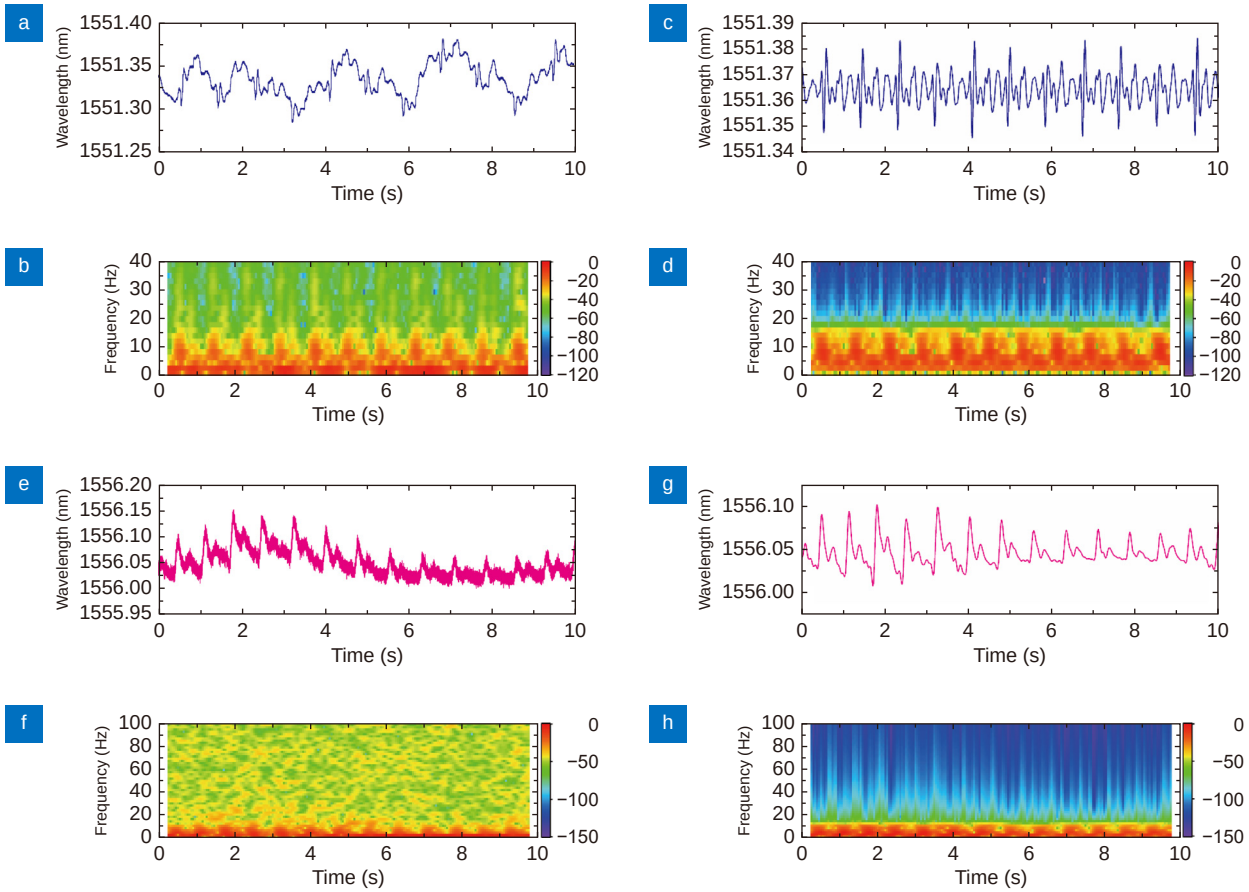

Fig. S4 | Signal preprocessing of BCG and pulse. (**a**) Raw time domain signal of BCG. (**b**) Time-frequency analysis of the raw BCG signal. (**c**) Time domain signal of BCG processed by a band-pass filter of 3-15 Hz. (**d**) Time-frequency analysis of the filtered BCG signal. (**e**) Raw time domain signal of pulse wave. (**f**) Time-frequency analysis of the raw pulse wave. (**g**) Time domain signal of pulse wave processed by a band-pass filter of 0.5-10 Hz. (**h**) Time-frequency analysis of the filtered pulse wave.

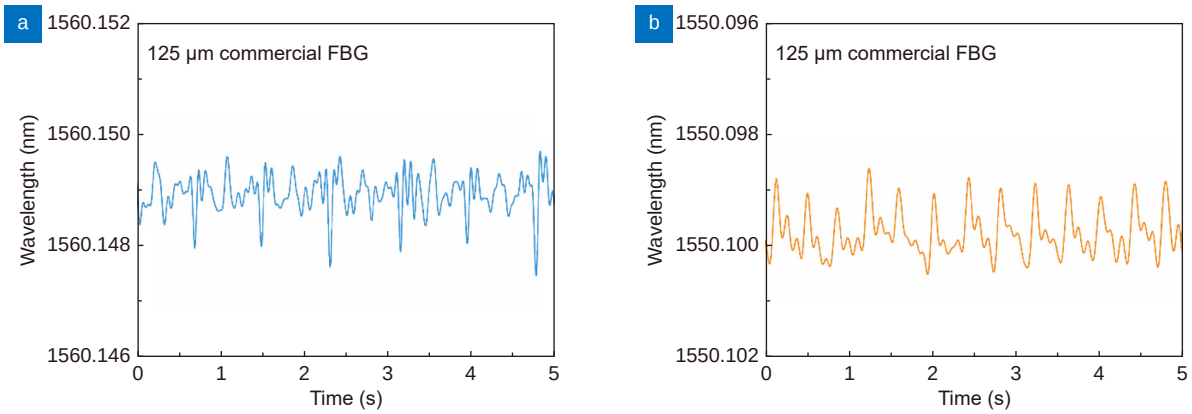

Fig. S5 | Comparison with commercial FBG. BCG signal (**a**) and pulse wave (**b**) detected by a commercial FBG with a diameter of 125 μm. Both the BCG signal and pulse wave are filtered by the same preprocessing methods.

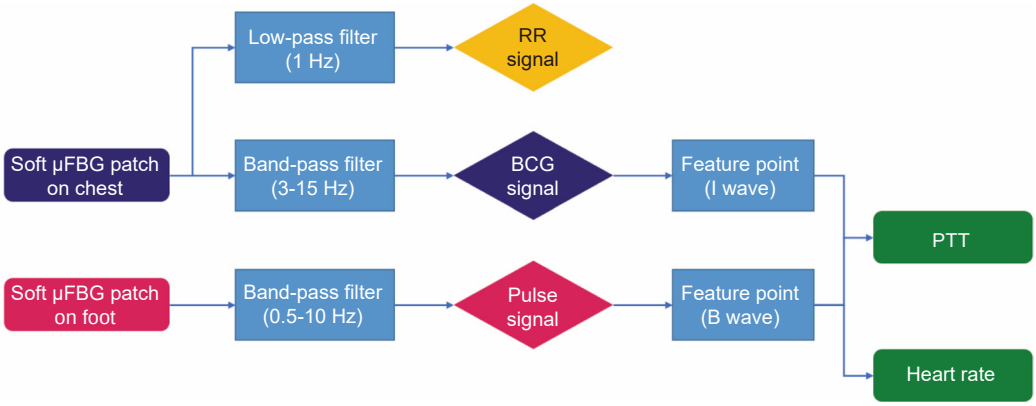

Fig. S6 | Flowchart of hemodynamic monitoring during exercise using soft μFBG group.

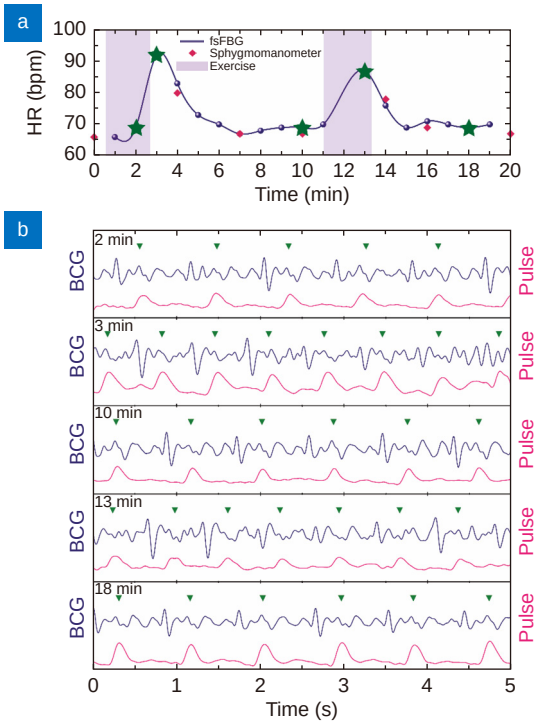

Fig. S7 | Heart rate (HR) calculation using soft μFBG group. (**a**) Comparison of HR acquired by the μFBG group (blue) and a commercial sphygmomanometer (red). (**b**) BCG signal and pulse wave detected by the soft μFBG group. The green triangle marks represent the cardiac cycle. The green stars in (a) illustrate the points in time of representive vital signals in (b).

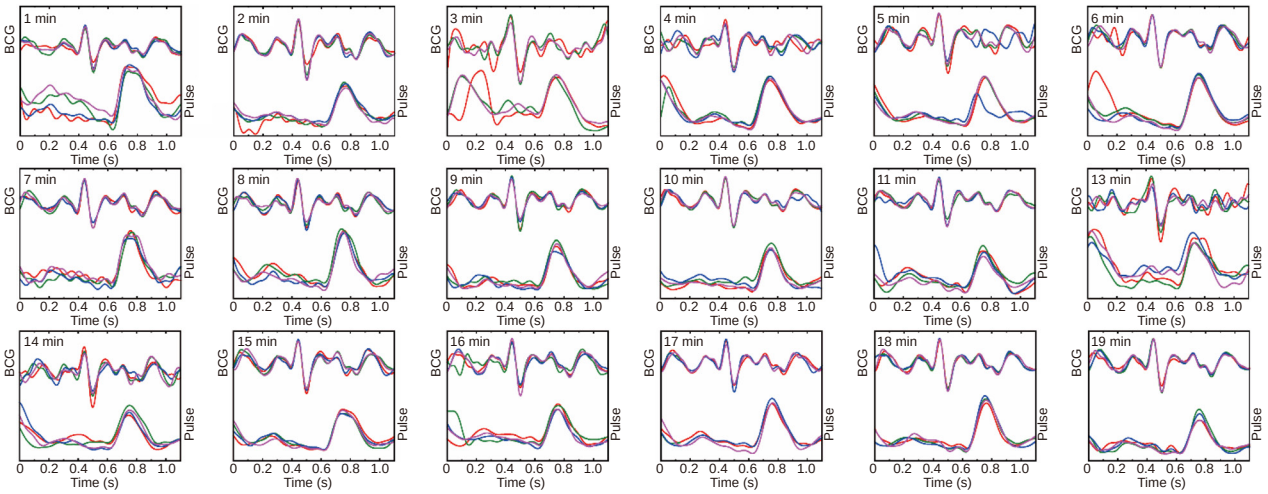

Fig. S8 | PTT calculation using soft μFBG group. Multiple groups of synchronized vital signals (BCG signal and pulse wave) are used to calculate the mean PTT per minute. To illustrate the subtle difference of the waveform and PTT, BCG signals are overlapped at the time point of I wave.

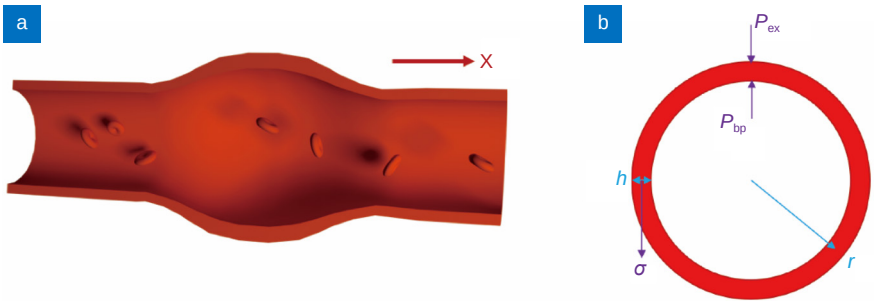

Fig. S9 | Model for analyzing the variation of BP and peripheral resistance. (**a**) Schematic diagram of the idea artery model. (**b**) The parameters used to analyze the relationship of PTT, BP, and peripheral resistance. *r*, *h*, and *σ*: radius, thickness, and stress of the blood vessel, respectively; P_{bp} and P_{ex}: blood pressure to the blood vessel and the external pressure by other tissue, respectively.

Section 3: Supplementary table

Table S1 | Comparison of the wearable devices based on the microfiber sensors.

Study	Sensing mechanism	Sensitivity	Functions	Multichannel sensing
Li et. al. [S2]	Intensity	0.83 kPa^{-1} for pressure	Pulse wave detection	X
Zhang et. al. [S3]	Intensity	1870 kPa^{-1} for pressure	Pulse wave detection, voice detection, and tactile sensing	X
Pan et. al. [S4]	Intensity	675 for strain	Respiration, arm motion, and body temperature sensing	X
Zhu et. al. [S5]	Intensity	257 for strain	Pulse wave detection and blood pressure monitoring	X
Zhao et. al. [S6]	Intensity	0.85 kPa^{-1} for pressure	Gesture recognition	X
This work	Wavelength	5.26 nm/N for pressure	Pulse wave and BCG signal detection	O

References

S1. Chen Y, Wen CY, Tao GC, Bi M, Li GQ. Continuous and noninvasive blood pressure measurement: a novel modeling methodology of the relationship between blood pressure and pulse wave velocity. *Ann Biomed Eng* **37**, 2222–2233 (2009).

S2. Li JH, Chen JH, Xu F. Sensitive and wearable optical microfiber sensor for human health monitoring. *Adv Mater Technol* **3**, 1800296 (2018).

S3. Zhang L, Pan J, Zhang Z, Wu H, Yao N et al. Ultrasensitive skin-like wearable optical sensors based on glass micro/nanofibers. *Opto-Electronic Advances* **3**, 19002201–19002207 (2020).

S4. Pan J, Zhang Z, Jiang CP, Zhang L, Tong LM. A multifunctional skin-like wearable optical sensor based on an optical micro-/nanofibre. *Nanoscale* **12**, 17538–17544 (2020).

S5. Zhu HT, Zhan LW, Dai Q, Xu B, Chen Y et al. Self‐assembled wavy optical microfiber for stretchable wearable sensor. *Adv Opt Mater* **9**, 2002206 (2021).

S6. Zhao L, Wu B, Niu Y, Zhu SK, Chen Y et al. Soft optoelectronic sensors with deep learning for gesture recognition. *Advanced Materials Technologies* **7**, 2101698 (2022).